Simulation-Assisted Methodology for the Design of Fiber-Based Dosimeters for a Variety of Radiation Environments

Damien Lambert, *Senior Member, IEEE*, Sylvain Girard, *Senior Member, IEEE*, Giovanni Santin, *Member, IEEE*, Marc Gaillardin, *Member, IEEE*, Adriana Morana, *Member, IEEE*, Arnaud Meyer, *Student Member, IEEE*, Jeoffray Vidalot, Jacques Baggio, Julien Mekki, Hugo Cintas, Olivier Duhamel, Claude Marcandella, and Philippe Paillet, *Fellow, IEEE*

***Abstract*— We present a simulation-assisted methodology for the design of point or distributed fiber dosimeters exploiting the linear dependence of the infrared (IR) radiation-induced attenuation (RIA) of a single-mode (SM) phosphosilicate optical fiber. We demonstrate by comparing Monte Carlo simulations and experiments at different irradiation facilities (X-rays, g-rays, protons, and atmospheric neutrons) that the sensitivity coefficient of this fiber is independent on the nature of particles and on dose rate, at least up to total ionizing doses (TIDs) in the order of 500 Gy. Our simulations allow us to simulate the dose deposited in the fiber core (and then the RIA levels) for the different classes of particles (photons, electrons, neutrons, protons, and heavy ions) and for different energy ranges. From these data and knowing the environments of targeted applications for the fiber optic dosimeters, we can discuss the different designs and achievable performance using this fiber. Examples are discussed with space applications, atmospheric balloon experiments, and fusion-devoted facilities.**

***Index Terms*— Dosimetry, Geant4, Monte Carlo simulations, optical fiber, radiation-induced attenuation (RIA).**

Manuscript received 21 September 2023; revised 22 January 2024, 27 February 2024, and 15 March 2024; accepted 15 March 2024. Date of publication 28 March 2024; date of current version 16 August 2024. *(Corresponding author: Damien Lambert.)*

Damien Lambert, Olivier Duhamel, Claude Marcandella, and Philippe Paillet are with the CEA, DAM, DIF, 91297 Arpajon, France (e-mail: damien.lambert@cea.fr; olivier.duhamel@cea.fr; claude.marcandella@cea.fr; philippe.paillet@cea.fr).

Sylvain Girard is with the Laboratoire Hubert Curien, UMR CNRS 5516, Université de Saint-Etienne, 42000 Saint-Etienne, France, and also with the Institut Universitaire de France (IUF), Ministère de l'Enseignement Supérieur et de la Recherche 75005 Paris, France (e-mail: sylvain.girard@univ-st-etienne.fr).

Giovanni Santin is with the European Space Agency (ESA), ESTEC, 2201 AZ Noordwijk, The Netherlands (e-mail: giovanni.santin@esa.int).

Marc Gaillardin is with the CEA, DAM, 46500 Gramat, France (e-mail: marc.gaillardin@cea.fr).

Adriana Morana, Arnaud Meyer, and Jeoffray Vidalot are with the Laboratoire Hubert Curien, UMR CNRS 5516, Université de Saint-Etienne, 42000 Saint-Etienne, France (e-mail: adriana.morana@univ-st-etienne.fr; arnaud.meyer@univ-st-etienne.fr; jeoffray.vidalot@univ-st-etienne.fr).

Jacques Baggio is with the CEA, DAM, CESTA, 33114 Le Barp, France (e-mail: jacques.baggio@cea.fr).

Julien Mekki and Hugo Cintas are with the CNES, 31400 Toulouse, France (e-mail: julien.mekki@cnes.fr; hugo.cintas@cnes.fr).

Color versions of one or more figures in this article are available at https://doi.org/10.1109/TNS.2024.3380318.

Digital Object Identifier 10.1109/TNS.2024.3380318

I. Introduction

TODAY, there is a strong interest in developing optical fiber radiation sensing, with either point or distributed sensors, able to monitor total ionizing dose (TID) in a variety of harsh environments. This interest is explained by the fact that these sensors have several advantages, especially when phosphorus-doped optical fibers are used as a sensitive element [1]. First, for most of on-Earth applications, it is possible to place the read-out electronics outside of the harsh environments associated with either radiation or electromagnetic constraints. To monitor TID, those sensors exploit the radiation-induced attenuation (RIA) mechanism, corresponding to an increase of the fiber attenuation with dose, caused by the generation of microscopic point defects in the fiber core and cladding, where the optical modes are propagating [1].

For P-doped optical fibers and at least up to a TID of 500 Gy (SiO_2) (50 krad), the RIA linearly increases with dose at wavelengths around 1550 nm, which corresponds to the third telecommunication window. This is explained by the particular properties of the P1 phosphorus-related point defect responsible for the RIA in this range of wavelengths [2], [3]. It is then possible for this class of optical fiber to define a radiation sensitivity coefficient (χ expressed in $dB{\cdot}km^{-1}{\cdot}Gy^{-1}$), allowing, after calibration, to deduce the TID by measuring the excess of optical losses. Second, it has been shown that in this infrared (IR, 1000–1800 nm) spectral range, the χ radiation sensitivity coefficient is mostly independent of dose rate or temperature during irradiation (−80 °C–120 °C), confirming the good potential of those fibers for dosimetry [4], [5].

Different techniques can be used to monitor the RIA and then deduce the TID. It is possible to design point sensors by using a fiber coil located at the precise position of interest and by combining a (mono- or multiwavelength) optical source and a detector (e.g., power meter, spectrophotometer). The main advantage of this approach is that by varying the fiber length, it is possible to adapt the accessible TID range, which is determined by the precision and dynamic range of the RIA measurement of the whole fiber length. Also, by changing the wavelength, higher χ can be accessible, although at the cost of

less robust dosimetry properties [6]. With a very long optical fiber (>km), as done for the LUMINA project [7], [8], [9], it becomes possible to measure TID levels as low as a few tens of μGy. Distributed sensors are another very interesting architecture of sensors: with a reflectometry technique, it is possible to measure the RIA along the optical fiber with typically a 1-m spatial resolution with optical time-domain reflectometers (OTDRs), and it is possible to achieve even better resolutions with optical frequency-domain reflectometer (OFDR). This technique is at the basis of the DOFRS system. As an example, CERN deployed it along their facilities or accelerators to monitor with OTDR the TID distribution [10], [11]. Finally, a very interesting property of those fibers is that their χ coefficient around 1550 nm appears to be almost independent on the type of particles; it is therefore possible to measure TID deposited by a variety of individual species or in mixed environments, as shown for X-ray and γ-ray photons [4], [5], [12], atmospheric neutrons [13], protons [4], or at the CHARM facility [14]. This clearly opens the way for the implementation of such sensors in very diverse environments for a variety of applications.

In this article, we detail our methodology, combining Geant4 Monte Carlo simulations and experiments to evaluate the potential of various architectures of fiber dosimeters for a given environment and mission profile. In order to perform such evaluation, one needs to estimate how the different particles forming the radiation environment of interest will deposit their energy in the selected fiber. Here, we use a phosphosilicate single-mode (SM) optical fiber, adapted to most of the currently available interrogators. After validating these simulations through benchmarking with experimental data from the literature or from additional new experiments, we illustrate how the output of these simulations can be used to evaluate the potential of fiber optic dosimeter architectures for different environments. In this work, we consider the three use cases of dosimeter: a stratospheric balloon experiment (from ground to 40 km), some specific space missions (a low Earth orbit Sun synchronous orbit, and interplanetary transit), and a fusion-devoted facility. These three examples have been taken as a possible complement to the dedicated dosimeters currently in use. A few sensor technologies are sensitive to a large diversity of particles (neutrons, protons, photons, etc.) in a large energy spectrum. The optical fiber dosimeter can be used as a complement to other sensors, such as scintillators and germanium detectors, with the rare advantage of having a unique calibration curve for the different particles. Only optical fiber technology enables distributed measurement, offering a multitude of measurement points for a single, very small sensing chain. These advantages make it possible to upgrade the existing detectors if the level to be detected is compatible with our technology. This level can be estimated using the simulation method presented in this article.

Our objective is to provide useful simulation outputs to estimate the dose deposited by a large variety of particles within the core of the radiosensitive optical fiber. Such calculations were done in the past in different bulk materials, for example, by Leray for Si [15]. His results are reported in Fig. 1, highlighting the fluence of a given particle (type and energy) needed to deposit 1 Gy(Si). Different simple numerical tools ("1-D"), such as SRIM [16] for protons, XCOM [17] for photons, or ESTAR [18] for electrons, can be used to estimate the energy depositions. In this article, we produce similar estimations, but we also use Geant4 3-D Monte Carlo simulations [19], [20], [21], [22] in order to consider the impact of the geometry of the radiosensitive phosphosilicate optical fiber on the dose deposition mechanisms.

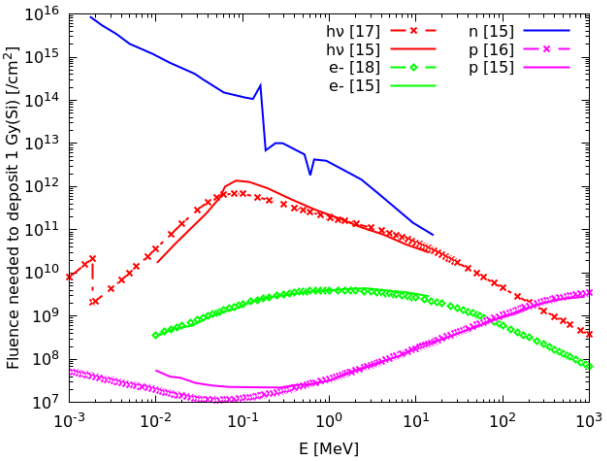

Fig. 1. Fluence needed to deposit 1 Gy or 100 rad in bulk silicon as a function of energy for different particles—historical approach with reference data extracted from [15], [16], [17], and [18].

II. Methods and Tools

In this section, we first present the selected optical fiber and then the Monte Carlo simulation setup used for this work. An important point is that the presented methodology can be adapted to other optical fiber structures, such as multimode phosphosilicate optical fibers with larger cores [23] or radiation sensitive aluminosilicate optical fibers [24].

A. Studied Phosphosilicate Optical Fiber

The tested optical fiber has been manufactured by iXblue (today Exail https://www.exail.com/) through a modified chemical vapor deposition (MCVD) process. This fiber is SM at 1310 and 1550 nm and has an acrylate coating. Its core, of ~8 μm diameter, is doped with phosphorus (10% wt), while its cladding (125 μm diameter) is made of pure silica (with some traces of fluorine). Its coating is made of an external ~250 μm diameter of acrylate (see [4] for more details).

This fiber has already demonstrated a very unique radiation response in the IR domain, allowing to perform point or distributed dosimetry measurements. Depending on the used interrogation technique, its radiation response is typically monitored between 1200 and 1700 nm (spectral measurements) or at some specific wavelengths (from 1310 to 1625 nm) when OTDR or laser combined with photodiode setups is involved.

B. Geant4-GRAS Modeling of Dose Deposition Within the Phosphosilicate Optical Fiber

In order to simulate the dose deposition mechanisms by various particles at different energies in this fiber, we use the

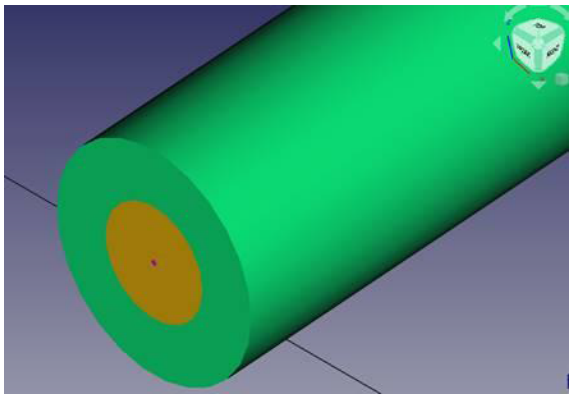

Fig. 2. P-doped SM optical fiber modeled with Geant4-GRAS. The fiber is exposed to an irradiation beam perpendicular to its propagation axis or an isotropic source. The fiber core is illustrated in red, its cladding in orange, and its coating in green.

TABLE I
ENERGY RANGE OF THE SIMULATED INCIDENT PARTICLES

Particle type	Energy Min	Energy Max
Photon	1 keV	100 MeV
Electron	1 keV	1 GeV
Neutron	0.1 meV	1 GeV
Ion	1 MeV/A	1 GeV/A

Geant4-GRAS model shown in Fig. 2. The dose deposited in the P-doped core is the main parameter to establish the fiber radiation sensitivity. It is well known that in SM optical fiber, the fundamental mode is also partially guided in the cladding, but it should be considered that, as core and cladding have very different radiation sensitivities, the mode re-equilibrium will strengthen the core contribution to this fiber response.

Geant4 (version 10.7.4) toolkit [19], [20], [21] has been used with the GRAS (version 5.2.1) [22] tool. Table I resumes the energy range simulated for each particle type. The physics used are em_standard_opt4 and FTFP_BERT_HP (not activated for photons and electrons), which are compliant with the incident particle species and energies and with the scale of the fibers.

As done in [25], we have used Freecad to design the geometry and materials of the fiber into a gdml file. As shown in Fig. 2, we consider that the optical fiber is exposed transversally (with respect to its propagation axis) to an incoming beam of particles. This configuration represents the ground irradiation tests performed on this fiber, which will be first benchmarked with the simulation outputs. Isotropic incidence responses have also been computed and are used for application to omnidirectional exposures (e.g., dosimeter in atmosphere or space). We present here only the response of one single layer of optical fiber, exposed to different radiation fields. If long fiber lengths are needed for the dosimeter, more realistic modeling considering the fiber coil structure and its impact on dose deposition should be considered. Obviously, for real applications, the impact of the dosimeter packaging on the dose deposited in the fiber core will also have to be considered for the final design of the dosimeter architecture.

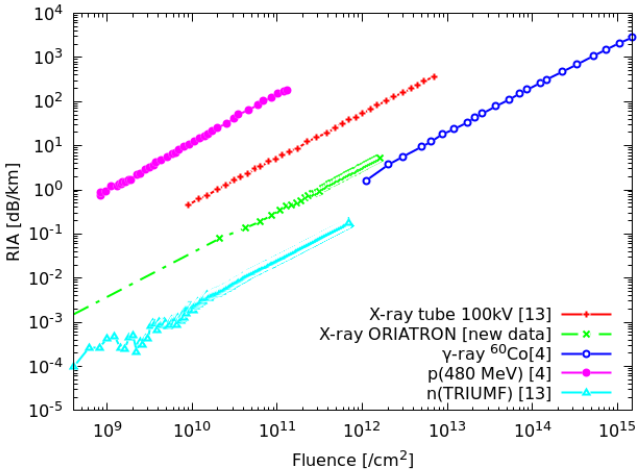

Fig. 3. RIA fluence dependence for five different irradiation campaigns. ORIATRON results are original, while the other results have been redrawn from [4] and [13].

TABLE II
TEST DESCRIPTION

Test type	Wavelength	Test Technique
X-ray tube (100 kV) and TRIUMF neutron [13]	1625 nm	Micro optical time domain reflectometer
^{60}Co [4]	1550 nm	Optical time domain reflectometer
ORIATRON [new data]	1532 nm	Erbium Doped fiber source with a photodiode
p(480 MeV) [4]	1550 nm	White light source with a spectrometer

III. EXPERIMENTAL AND MODELING RESULTS

In this section, we first report the available experimental results, both from literature and from new irradiation campaigns regarding the IR-RIA around 1550 nm versus fluence, measured using different setups at different facilities. Then, we present the Monte Carlo simulations output regarding the dose deposited within the same optical fiber.

A. Experimental Results

The dependence of the RIA on particle fluence for different beams is illustrated in Fig. 3. As the measurements were performed with a variety of experimental setups and at slightly different IR wavelengths, Table II resumes the main characteristics of the tests. Different techniques can lead to uncertainty between measurements. However, we assume that the uncertainty induced by various techniques and probing wavelengths [12] is consistent with the dosimetry of the different installations. Moreover, the statistical uncertainty induced by a low number of deposit-inducing events also produces uncertainty in the measurement. RIA results at low neutron fluence ($<10^{10}$ cm^{-2}) illustrate perfectly the uncertainty induced by low statistics.

RIA linearly increases with particle fluence at different rates for the different particles. Losses are reported here without ORIATRON beam filtering as it was shown that Al filters change the dose deposited in the fiber [26].

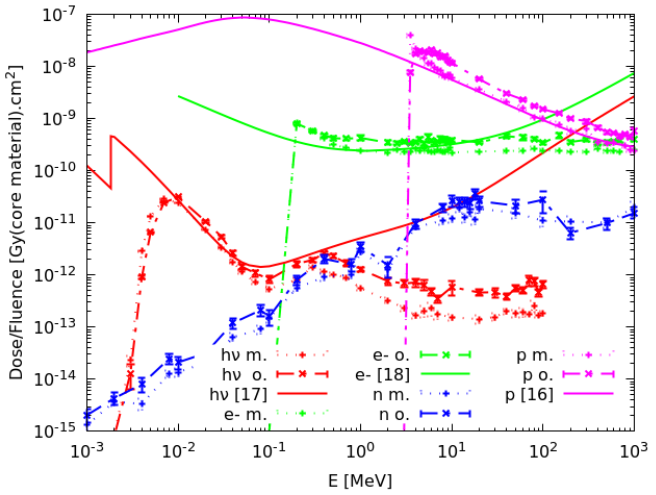

Fig. 4. Dose–fluence ratios calculated for photons (hν), electrons (e-), protons (p), and neutrons (n) for the tested P-doped SM optical fiber. Two cases are considered: a monodirectional irradiation beam (m.) and an omnidirectional bream (o.). Comparison to database references: XCOM, ESTAR, and SRIM [16], [17], [18].

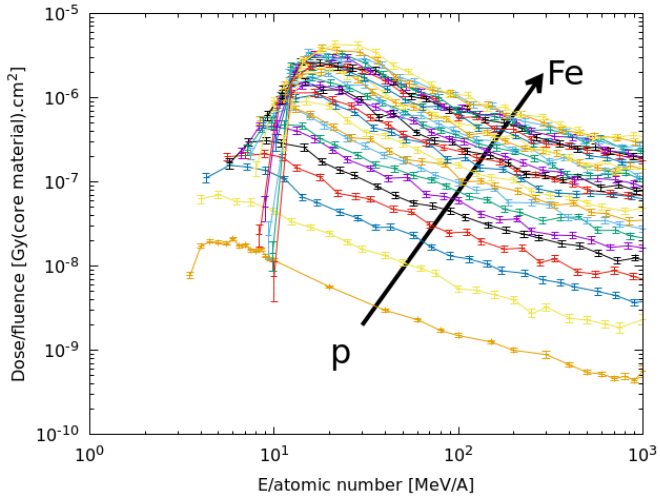

Fig. 5. Dose–fluence ratios calculated for all the ions lighter than iron. An omnidirectional beam is considered.

B. Geant4-GRAS Simulation Results

Fig. 4 displays the simulation results of dose deposition within the fiber core for electrons, neutrons, protons, and photons. From this figure, one can directly deduce the fluence of monoenergetic particles needed to deposit one Gy within the fiber core under test, as shown in Fig. 1. Two different irradiation cases are considered: first, a monodirectional irradiation beam (corresponding to the usual ground tests) and, second, an omnidirectional irradiation condition that could be encountered in real application cases. The provided curves can also be used to estimate the dose deposition from more complex mixed-field environments combining a variety of particle species at different energies. Some simulations in air have been done previously using FLUKA in order to compare the doses measured by this fiber with those calculated by CERN at different locations of the CHARM Facility [10].

Our results show that for electrons, photons, and protons, there is an energy threshold, below which the particle energy is too low to reach the fiber core and therefore cannot contribute to the deposited dose in this radiosensitive volume. This threshold depends on the fiber characteristics (core, cladding, and coating size), its packaging (fiber coil, etc.), and eventual dosimeter packaging. These thresholds are of ∼2 keV for photons, ∼100 keV for electrons, and ∼3 MeV for protons, for the considered bare SM optical fiber. At low energy, the neutron sensitivity is low, but no threshold is observed. For neutrons, deposition in the core is mainly induced by secondary particles from nuclear reactions with the atoms in the optical fiber. The core of the fiber is an amorphous structure that is by nature less sensitive to displacement damages than the crystalline structures widely used in electronics. Our results suggest that for our optical fibers, under neutron irradiations at low fluences, for the other particles, ionizing dose remains the main effect driving the RIA level and kinetics. We observed that, as a general rule, the omnidirectional irradiation source leads to a slightly higher deposited dose, whatever the nature of the particles. This is due to the combination of the angle of incidence and the mean free path of the particles.

Both results are also consistent with the estimates from databases illustrated in Fig. 1 (e.g., XCOM, ESTAR, and SRIM) when the electronic equilibrium for deposition is reached, and the dimension of the fiber is of the same order of magnitude as the particle mean free path.

Although no radiation test results are yet available for heavy ions, their contribution will have to be considered in space, typically originating from galactic cosmic rays (GCRs) and potentially also in solar particle events. With the same simulation methodology, we have obtained the fiber-dose responses for a variety of heavy ion species. These results are reported in Fig. 5. The ion curves all have the same shape. Above a threshold energy, the deposit increases to a maximum and decreases thereafter. The deposition maximum and threshold energy increase with the ion's atomic number.

IV. Discussion of Simulation Results

In this section, we first demonstrate that those simulations allow deriving the RIA levels caused by the particles of different types and of varying energies. Subsequently, we used those validated simulation results to evaluate the feasibility of developing fiber dosimeters for different application cases.

A. Study of Radiation Sensitivity Coefficient and Its Dependence on Particle's Type and Energy

Fig. 6 shows the experimental results combined with simulations to present the RIA as a function of dose in the fiber core. We see the linear dependence of the RIA versus deposited dose in the core for different beams. Where statistics are sufficient, experimental data are between 3 and 5 $dB \cdot km^{-1} \cdot Gy^{-1}$. Considering all uncertainties, the coefficient of 4 $dB \cdot km^{-1} \cdot Gy^{-1}$ allows a good fit for all data. To explain the observed difference, one should consider that those data points have been obtained using setups operating at slightly different wavelengths and different dose rates and also that for some of the experiments, fiber coils have been used

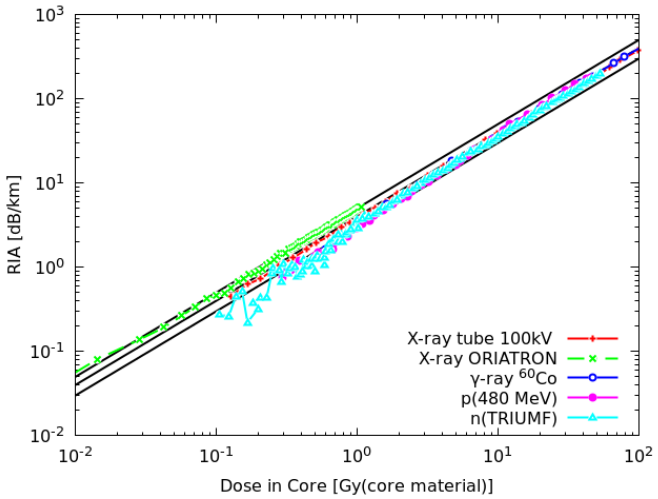

Fig. 6. RIA as a function of TID in the fiber core from the five irradiations campaign data of Fig. 1 and simulated radiation sensitivity coefficients expressed in dB·km^{-1}·Gy^{-1}. The 3-, 4-, and 5-dB·km^{-1}·Gy^{-1} linear fits have been added in black curve. Considering all the measurement uncertainties, the 4 dB·km^{-1}·Gy^{-1} is the best fit curve.

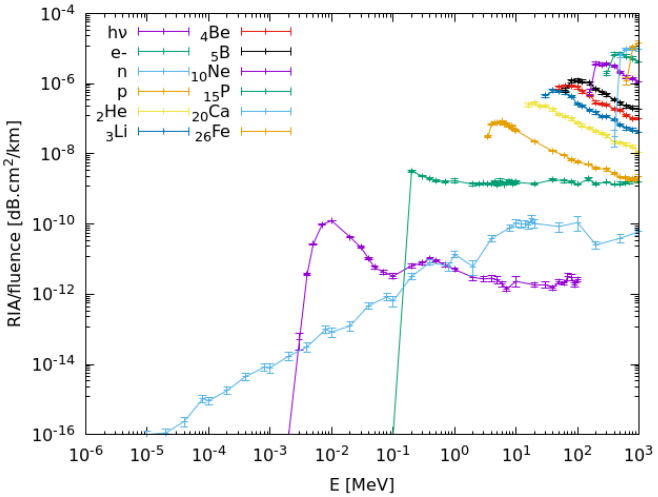

Fig. 7. RIA–fluence ratio as a function of energy for photons, electrons, neutrons, protons, and heavy ions for the studied optical fiber in an omnidirectional particle environment. The figure shows the results for a few ions. The various curves are arranged in order of atomic number.

(e.g., for neutron testing) for which the dose calculation needs to be improved in the future.

B. RIA–Fluence Ratio for Different Particle's Types and Energies

As seen in Section II-A, as a first approximation, we can consider the radiation sensitivity coefficient χ [χ(particle, E) = 4 dB·km^{-1}·Gy^{-1} around 1550 nm] independent of the species of the particle causing the dose deposition in the P-doped SM optical fiber core. In order to facilitate the estimation of the feasibility to use fiber dosimetry in a given environment, it is then possible to calculate the RIA per unit fluence. The obtained results are illustrated in Fig. 7, giving those coefficients for protons, neutrons, photons, electrons, and heavy ions. For clarity, for heavy ions, the simulation curves have been cut at their threshold energies (which is the mean path length to reach the core fiber). We have a first dataset for a monodirectional source and a second for an omnidirectional source. Depending on the application and the type of source, either monodirectional or omnidirectional results are used. Based on these curves, one can estimate for this particular fiber the IR-RIA for a given radiation environment, also in case of mixed-field, through the following formula:

$$\mathrm{RIA} = \sum_{\text{particle}} \int \chi(\text{particle}, E) \frac{\text{Dose}(\text{particle}, E)}{\phi(\text{particle}, E)} \times \frac{d\phi(\text{particle}, E)}{dE} dE \quad (1)$$

C. Estimating the Feasibility of Dosimetry Measurements in Different Application Cases

Knowing the radiation environments, the developed methodology allows calculating the expected RIA for a given irradiation condition. Once the RIA levels are determined, one can determine if point or distributed dosimeter architectures can be tuned to monitor the dose levels of this environment.

We apply this method to different application cases—environments as follows.

- Atmospheric environment at various altitudes.
- Space missions.
- Fusion-related facilities.

Knowing the detection level of RIA and the integration time, such a calculation allows: 1) establishing the feasibility of performing fiber-based dosimetry in such environments; 2) determining the performance of the dosimeter in terms of minimum dose, interrogation techniques, acquisition time, and dynamic range; and 3) optimizing the sensor architecture: fiber length, shielding, and so on.

The detection level of the RIA is strongly related to the choices of optoelectronic equipment selected for the loss measurement and also to the selected integration time for those measurements. Today, in our tests, we have shown that solutions exist to measure the RIA with a 5-mdB resolution for both point and distributed sensor architectures. As the radiation-induced losses linearly depend on the fiber length, this parameter could be adjusted up to several kilometers for point sensors optimized for low dose monitoring (e.g., for the LUMINA dosimeter [7], [8]). For this class of dosimeter, the maximum dose will be fixed by the dynamic range of the RIA measurements (today, the dynamic range of 50 dB is possible). In the case of distributed measurements, the spatial resolution will be limited by the length needed to reach 5 mdB, while the sensing length will be, at the first order, fixed by the dynamic range of the reflectometer [12].

1) Atmospheric Balloons: As it is commonly known, the atmospheric environment at altitudes above a few kilometers is composed mainly of neutrons and protons [27]. Different models exist. Among them, we have selected MAIRE [28] and RAMSEES [29], [30], which give the necessary data for our process. Due to these tools, we have the neutron and proton energy fluxes at different altitudes (between 4 and 20 km for MAIRE and between 0 and 40 km for RAMSEES). By combining the spectra and (1) formula, we can estimate the dose rate in the fiber.

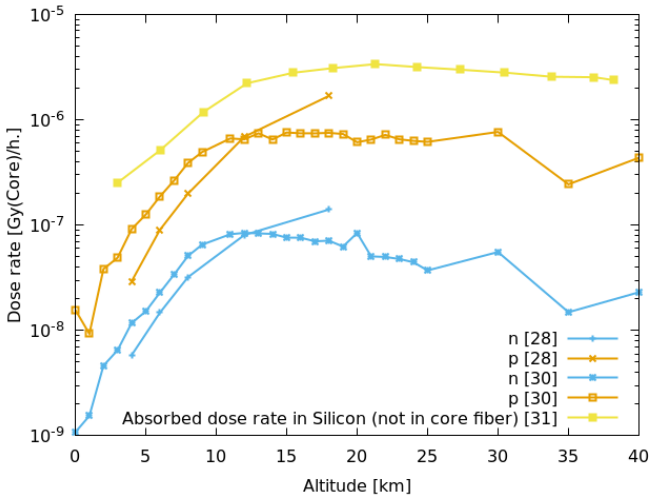

Fig. 8. Dose rate in core as a function of altitude induced by neutron (n) and proton (p) for the two spectrum references [28], [29], [30], [31].

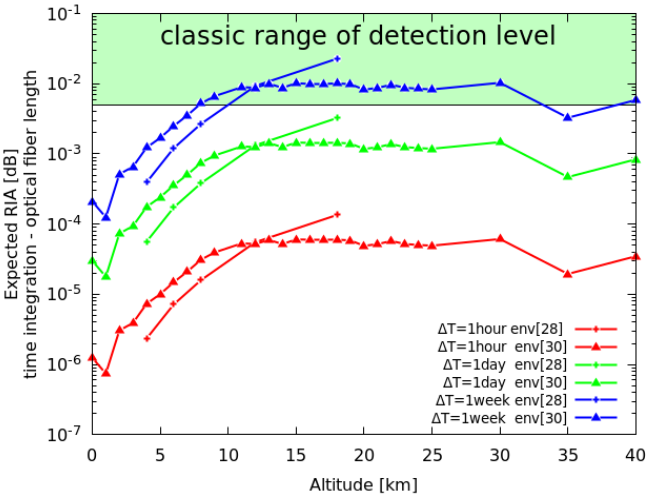

Fig. 9. Expected RIA as a function of altitude for three integration times—and an optical fiber length of 20 km for the two selected models in atmospheric environment.

As shown in Fig. 8, the dose rate seen by the fiber core is mainly induced by the protons, although the neutron flux may be higher. The selected fiber is more sensitive to protons than neutrons. The two spectra models give the results of the same order of magnitude. Hands et al. [31] illustrate the absorbed dose in a silicon detector for comparison. The dose detected in the fiber core is lower than in [31], which has been optimized at the dose equilibrium. The balloons' trajectories are different and are therefore characterized by different environments. A dedicated study of the fiber packaging (material surrounding the fiber) could be done in the future to optimize the dose deposition into its core and enhance its sensitivity.

Fig. 9 shows the RIA results for different integration times and a long fiber length of 20 km. This chosen fiber length (20 km) corresponds to a maximum feasibility value of what can be conventionally used today. The three integration times selected already correspond to large durations for a balloon experiment. With the selected long fiber coil, to reach a detectable RIA, we need an integration time of the order of a

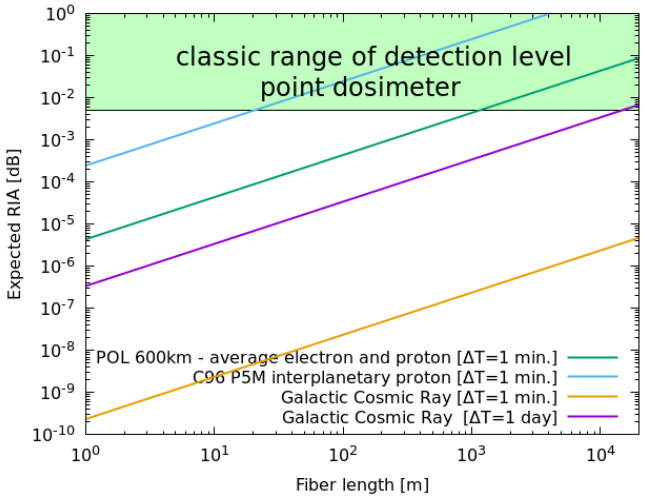

Fig. 10. Expected RIA as a function of fiber length for three types of environment (no shield and 2π sr): "POL 600-km" trapped electrons and protons, Creme96 Peak 5-min protons, and GCR protons [32], [33], [34], [35], [36] and integration time.

week and then a long flight duration. These various constraints may be considered too restrictive for a realistic operational case. For this environment, a more sensitive fiber (or the same optical fiber operated at a different wavelength, where its χ is larger) will have to be identified to reach RIA levels that could be detected over a larger range of experimental durations and fiber lengths.

2) Space Scenarios: The same method can be used for the various components of the space environment such as in the following scenarios.

1) Average trapped electrons and protons (AE8; AP8 models [32], [33]) for a near-polar-Sun-synchronous low Earth orbit (here indicated as POL) at 600-km altitude (AE9; AP9 newer models can also give more up to date spectra [34]).
2) A peak solar proton environment in interplanetary space (CREME96 peak 5 min: P5M [35]).
3) GCRs in interplanetary space (Solar minimum, ISO 15390 model [36]).

We have considered the case of a detector placed outside on the satellite surface (no shielding and a 2π sr solid angle). As shown in Fig. 10, we can see that the space environments considered here would induce very different levels of RIA. The Creme96 P5M can be easily detected with a few tens of meters of fiber at 1-min sampling, while the POL 600-km environment made up of electrons and protons would require the lengths of about 1 km. For the studied fiber, GCR detection is more difficult: heavy ions from GCRs have low fluxes and are not necessarily compatible with the fiber coil structure. In this case, to detect GCR as for the atmospheric environment, one could imagine to exploit another type of fiber dosimeters based on radioluminescence that could detect lower flux of particles [37]. GCR detection through RIA will probably require a dedicated fiber with higher detection efficiency and dedicated geometry (such as tapered optical fibers [39]) and materials. Solar peak protons can be detected with a 1-min resolution with a fiber length of around 1 km, that is clearly

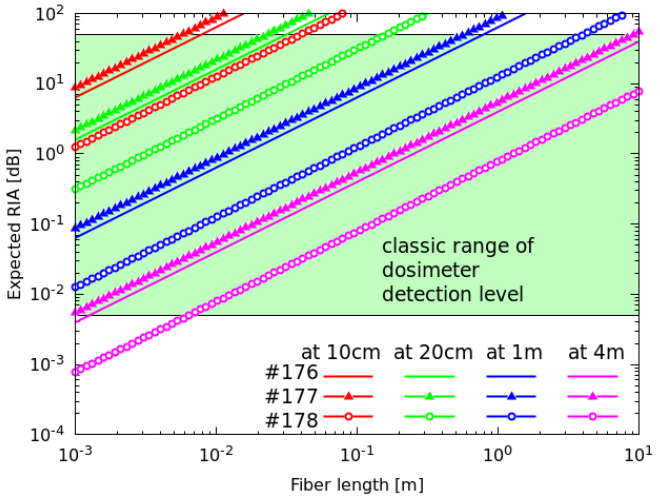

Fig. 11. Expected RIA as a function of fiber length for three configurations at the PETAL facility. Four distances from the target are explored: 10 cm, 20 cm, 1 m, and 4 m.

realistic with a point sensor, such as LUMINA. For long-term measurement (hours and days), one could envisage to design distributed dosimeters too.

3) Fusion Facilities: Optical fibers can also be used for dosimetry instrumentation in large-scale physics facilities. We apply the method to the PETAL facility at the Laser Megajoule in France [40] that is devoted to the study of fusion by inertial confinement. Depending on the target, PETAL can produce a pulsed mixed environment of electrons, protons, and ions (C and O). Based on the fluences and the spectra described in [40], we estimate the induced RIA of three past shots numbered #176, #177, and #178 at this facility for different fiber lengths (from 1 to 10 m) and for increasing distances for the radiation source (from 10 cm to 4 m). The given RIA results from the contributions from the electron, proton, and C and O ions. Our calculations show that the C and O ions do not have sufficient energy to reach the fiber core and then do not contribute to the dose deposition and RIA in the fiber core. The fluence and resulting RIA contribution from the electrons are lower than those of protons. As a result, the fiber degradation resulting from the PETAL shots is mainly induced by protons.

Fig. 11 summarizes the RIA responses of the different configurations. As we can see, the associated doses lead to losses easily exceeding the 5-mdB threshold (minimum of the classic range of dosimeter detection level) even for short lengths of fiber. This means that the minimum detection threshold could be reached with conventional instrumentation for both point and distributed sensing. For distances close to the target (10 and 20 cm), the RIA of a fiber a few centimeter long is greater than 50 dB. This high value will quickly saturate the conventional architectures. At 1-m distance and with fiber lengths of a few centimeters, the RIA amplitude should be fully compatible with conventional point sensor architecture (5 mdB, 50 dB of dynamic). At 4 m, it should be possible to do distributed dosimetry, potentially with an OFDR offering better spatial resolution than OTDR but at the cost of a reduced dynamic range [38].

V. Conclusion

We present a methodology combining experiments and Geant4 Monte Carlo simulations to evaluate the potential of dosimeters exploiting the RIA in an SM phosphosilicate optical fiber for neutrons, photons, electrons, protons, and heavy ions irradiations.

This method has been used in a variety of environments as follows:

1) atmospheric environment, where the chosen fiber without a dedicated package appears to be not sensitive enough to give realistic RIA detection;
2) space, where the results show that fiber dosimetry is compliant with realistic scenarios;
3) fusion-related facility, where fiber RIA measurements are possible in most application use cases.

This method combines a few experimental results with Monte Carlo calculations to estimate the response levels of fiber-based dosimeters. In the case of the fusion application, both point or distributed dosimeters exploiting the RIA response of the studied fiber can be designed. For space applications, fiber dosimetry is also fully compatible. In the future and depending on the radiative component of interest, the system could be made more complex to include a combination of several optical fibers with adapted prefilters to offer a certain level of discrimination between the different particles. Finally, in the case of atmospheric balloon applications, the studied solution needs to be developed and optimized to deposit more TID in the fiber and increase the level of RI, because it appears to be close to the detection limit even for an experiment duration of one week. A prefilter adaptation study, considering the incident energy spectrum, could enable the particle detection to be optimally sized with respect to the fiber characteristics. This will be investigated in the future.

References

[1] S. Girard et al., "Radiation effects on silica-based optical fibers: Recent advances and future challenges," *IEEE Trans. Nucl. Sci.*, vol. 60, no. 3, pp. 2015–2036, Jun. 2013, doi: 10.1109/TNS.2012.2235464.

[2] D. L. Griscom, E. J. Friebele, K. J. Long, and J. W. Fleming, "Fundamental defect centers in glass: Electron spin resonance and optical absorption studies of irradiated phosphorus-doped silica glass and optical fibers," *J. Appl. Phys.*, vol. 54, no. 7, pp. 3743–3762, Jul. 1983, doi: 10.1063/1.332591.

[3] S. Girard et al., "Overview of radiation induced point defects in silica-based optical fibers," *Rev. Phys.*, vol. 4, Nov. 2019, Art. no. 100032, doi: 10.1016/j.revip.2019.100032.

[4] D. D. Francesca et al., "Qualification and calibration of single-mode phosphosilicate optical fiber for dosimetry at CERN," *J. Lightw. Technol.*, vol. 37, no. 18, pp. 4643–4649, Sep. 15, 2019, doi: 10.1109/JLT.2019.2915510.

[5] A. Morana et al., "Operating temperature range of phosphorous-doped optical fiber dosimeters exploiting infrared radiation-induced attenuation," *IEEE Trans. Nucl. Sci.*, vol. 68, no. 5, pp. 906–912, May 2021, doi: 10.1109/TNS.2021.3053164.

[6] L. Weninger et al., "Calibration in the visible and infrared domains of multimode phosphosilicate optical fibers for dosimetry applications," *IEEE Trans. Nucl. Sci.*, vol. 70, no. 8, pp. 1908–1916, Aug. 2023, doi: 10.1109/TNS.2023.3252941.

[7] F. Clément et al., "LUMINA, a fiber optic dosimeter aboard the ISS," presented at the 73rd Int. Astron. Congr. (IAC), Paris, France, Sep. 2022.

[8] D. Di Francesca et al., "Low radiation dose calibration and theoretical model of an optical fiber dosimeter for the international space station," *Appl. Opt.*, vol. 62, no. 16, p. E43, Jun. 2023, doi: 10.1364/ao.483560.

[9] M. Roche et al., "Solar particle event detection with the LUMINA optical fiber dosimeter aboard the international space station," *IEEE Trans. Nucl. Sci.*, early access, Feb. 20, 2024, doi: 10.1109/TNS.2024.3368137.

[10] D. Di Francesca et al., "Distributed optical fiber radiation sensing in the proton synchrotron booster at CERN," *IEEE Trans. Nucl. Sci.*, vol. 65, no. 8, pp. 1639–1644, Aug. 2018, doi: 10.1109/TNS.2018.2818760.

[11] K. Bilko et al., "CERN super proton synchrotron radiation environment and related radiation hardness assurance implications," *IEEE Trans. Nucl. Sci.*, vol. 70, no. 8, pp. 1606–1615, Aug. 2023, doi: 10.1109/TNS.2023.3261181.

[12] A. Meyer et al., "Toward an embedded and distributed optical fiber-based dosimeter for space applications," *IEEE Trans. Nucl. Sci.*, vol. 70, no. 4, pp. 583–589, Apr. 2023, doi: 10.1109/TNS.2022.3226194.

[13] S. Girard et al., "Atmospheric neutron monitoring through optical fiber-based sensing," *Sensors*, vol. 20, no. 16, p. 4510, Aug. 2020, doi: 10.3390/s20164510.

[14] D. Di Francesca et al., "Dosimetry mapping of mixed-field radiation environment through combined distributed optical fiber sensing and FLUKA simulation," *IEEE Trans. Nucl. Sci.*, vol. 66, no. 1, pp. 299–305, Jan. 2019, doi: 10.1109/TNS.2018.2882135.

[15] J. L. Leray, "Contribution à l'étude des phénomènes induits par les rayonnements ionisants dans les structures à effet de champ Au silicium Ou à l'arseniure de gallium utilisées en microelectronique," Ph.D. dissertation, Université de Paris Sud, Centre d'Orsay, France, 1989.

[16] J. Ziegler. (Dec. 2013). *The Stopping and Range of Ions in Matter*. [Online]. Available: https://www.srim.org

[17] M. J. Berger et al., "XCOM: Photon cross sections database NIST standard reference database 8 (XGAM)," Tech. Rep., Nov. 2010, doi: 10.18434/T48G6X.

[18] M. J. Berger et al., "Stopping-power & range tables for electrons, protons, and helium ions—NIST standard reference database 124," Tech. Rep., 2017, doi: 10.18434/T4NC7P.

[19] J. Allison et al., "GEANT4 developments and applications," *IEEE Trans. Nucl. Sci.*, vol. 53, no. 1, pp. 270–278, Feb. 2006, doi: 10.1109/TNS.2006.869826.

[20] S. Agostinelli et al., "GEANT4—A simulation toolkit," *Nucl. Instrum. Methods Phys. Res. A, Accel. Spectrom. Detect. Assoc. Equip.*, vol. 506, no. 3, pp. 250–303, Jul. 2003, doi: 10.1016/s0168-9002(03)01368-8.

[21] J. Allison et al., "Recent developments in GEANT4," *Nucl. Instrum. Methods Phys. Res. A, Accel. Spectrom. Detect. Assoc. Equip.*, vol. 835, pp. 186–225, Nov. 2016, doi: 10.1016/j.nima.2016.06.125.

[22] G. Santin, V. Ivanchenko, H. Evans, P. Nieminen, and E. Daly, "GRAS: A general-purpose 3-D modular simulation tool for space environment effects analysis," *IEEE Trans. Nucl. Sci.*, vol. 52, no. 6, pp. 2294–2299, Dec. 2005, doi: 10.1109/TNS.2005.860749.

[23] S. Girard, Y. Ouerdane, C. Marcandella, A. Boukenter, S. Quenard, and N. Authier, "Feasibility of radiation dosimetry with phosphorus-doped optical fibers in the ultraviolet and visible domain," *J. Non-Crystalline Solids*, vol. 357, nos. 8–9, pp. 1871–1874, Apr. 2011, doi: 10.1016/j.jnoncrysol.2010.11.113.

[24] A. Alessi et al., "Near-IR radiation-induced attenuation of aluminosilicate optical fibers," *Phys. Status Solidi, A*, vol. 218, no. 15, Aug. 2021, doi: 10.1002/pssa.202000807.

[25] D. Lambert et al., "TID effects induced by ARACOR, ^{60}Co, and ORIATRON photon sources in MOS devices: Impact of geometry and materials," *IEEE Trans. Nucl. Sci.*, vol. 68, no. 5, pp. 991–1001, May 2021, doi: 10.1109/TNS.2021.3074711.

[26] M. Gaillardin et al., "Investigations on ionizing dose deposition in thin-layered devices: Sample-to-sample variability and electronic equilibrium dependence," *IEEE Trans. Nucl. Sci.*, vol. 70, no. 8, pp. 2027–2033, Aug. 2023, doi: 10.1109/TNS.2023.3239950.

[27] G. Santin, P. Truscott, R. Gaillard, and R. G. Alía, "Radiation environments: Space, avionics, ground and below," in *Proc. RADECS*, Geneva, Switzerland, 2017, p. 142.

[28] F. Lei, S. Clucas, C. Dyer, and P. Truscott, "An atmospheric radiation model based on response matrices generated by detailed Monte Carlo simulations of cosmic ray interactions," *IEEE Trans. Nucl. Sci.*, vol. 51, no. 6, pp. 3442–3451, Dec. 2004, doi: 10.1109/TNS.2004.839131.

[29] H. Cintas et al., "RAMSEES: A model of the atmospheric radiative environment based on GEANT4 simulation of extensive air shower," *Aerospace*, vol. 10, no. 3, p. 295, Mar. 2023, doi: 10.3390/aerospace10030295.

[30] H. Cintas et al., "Impact of ground material and space protons direction on neutron flux in atmosphere," presented at the Nucl. Space Radiat. Effect Conf., Kansas City, MI, USA, Jul. 2023.

[31] A. D. P. Hands, K. A. Ryden, and C. J. Mertens, "The disappearance of the Pfotzer–Regener maximum in dose equivalent measurements in the stratosphere," *Space Weather*, vol. 14, no. 10, pp. 776–785, Oct. 2016, doi: 10.1002/2016sw001402.

[32] D. M. Sawyer and J. I. Vette, "AP-8 trapped proton environment for solar maximum and solar minimum," NASA, Greenbelt, MD, USA, Tech. Rep. TM-X-72605, 1976.

[33] J. I. Vette, "The AE-8 trapped electron model environment," NASA, Greenbelt, MD, USA, Tech. Rep. WDC-A-R&S 91-24, 1991.

[34] W. R. Johnston, T. P. O'Brien, S. L. Huston, T. B. Guild, and G. P. Ginet, "Recent updates to the AE9/AP9/SPM radiation belt and space plasma specification model," *IEEE Trans. Nucl. Sci.*, vol. 62, no. 6, pp. 2760–2766, Dec. 2015, doi: 10.1109/TNS.2015.2476470.

[35] A. J. Tylka et al., "CREME96: A revision of the cosmic ray effects on micro-electronics code," *IEEE Trans. Nucl. Sci.*, vol. 44, no. 6, pp. 2150–2160, Dec. 1997, doi: 10.1109/23.659030.

[36] *Space Environment (Natural and Artificial)—Galactic Cosmic Ray Model*, Standard ISO 15390:2004(E), 2004.

[37] S. Girard et al., "X-rays, γ-rays, and proton beam monitoring with multimode nitrogen-doped optical fiber," *IEEE Trans. Nucl. Sci.*, vol. 66, no. 1, pp. 306–311, Jan. 2019, doi: 10.1109/TNS.2018.2879791.

[38] A. V. Faustov et al., "Application of phosphate doped fibers for OFDR dosimetry," *Results Phys.*, vol. 6, pp. 86–87, Jan. 2016, doi: 10.1016/j.rinp.2016.02.001.

[39] F. Fricano et al., "Investigation of the dosimetry properties of radioluminescent nitrogen-doped tapered optical fibers," *IEEE Sensors J.*, vol. 23, no. 22, pp. 27300–27306, Nov. 2023, doi: 10.1109/JSEN.2023.3316773.

[40] D. Raffestin et al., "Enhanced ion acceleration using the high-energy petawatt PETAL laser," *Matter Radiat. Extremes*, vol. 6, no. 5, Aug. 2021, Art. no. 056901, doi: 10.1063/5.0046679.